



ASME Accepted Manuscript Repository

Institutional Repository Cover Sheet

First

Last

ASME Paper Title: An Experimental and Numerical Study of Added Mass and Damping for Side-by-Side Plates in Oscillatory Flow

Authors: Frøydis Solaas, Fredrik Mentzoni, Mia Abrahamsen-Prsic, Trygve Kristiansen

ASME Journal Title: Journal of Offshore Mechanics and Arctic Engineering.

Volume/Issue _143/1_ Date of Publication (VOR* Online) _2020-07-01_

ASME Digital Collection URL: <https://doi.org/10.1115/1.4047451>

DOI: <https://doi.org/10.1115/1.4047451>

*VOR (version of record)

Note: Snapshot PDF is the proof copy of corrections marked in EditGenie, the layout would be different from typeset PDF and EditGenie editing view.

Author Queries & Comments:

Q1 : Reminder – the ASME Copyright Agreement that was signed by all authors includes the following: “You have the right to enter into this Copyright Form and to make the assignment of rights to ASME. If the Paper contains excerpts from other copyrighted material (including without limitation any diagrams, photographs, figures or text), you have acquired in writing all necessary rights from third parties to include those materials in the Paper, and have provided appropriate credit for that third-party material in footnotes or in a bibliography.” As required, ASME may contact the authors to obtain a copy of the written permission. Any content obtained from the web and included in the paper may require written permission and appropriate credit if it is copyrighted content. If copyright status cannot be determined, this content should not be included in the paper. Please note the figures in this proof are low resolution, the final paper will publish with all figures as 300 dpi.

Response: Resolved

Q2 : Please check and approve the edits made to the article title.

Response: Resolved

Q3 : Keywords given in Starter xml have been used, please confirm if this is correct.

Response: “Please be so kind to use the following key-words: Added mass and damping; Subsea structures; Side-by-side plates.

Q4 : Please note that figure citations are in sequential order and hence this has been renumbered. Kindly check if this is appropriate.

Response: Resolved

Q5 : Please provide the city of the publisher Refs. 1–3.

Response: Resolved

Q6 : Please provide date of conference and page range for Ref. 6

Response: Please note that the page number is 78315: 1 - 11.

Q7 : Please provide the issue number in Refs. 6, 10, and 12.

Response: Please notice that, while the volume number is, as stated, 84, the Journal does not provide the issue number. The papers within a volume are classified either as “Regular papers” or “Special issue”. Since the present reference belongs to “regular papers”, stating the issue might be redundant.

Q8 : Please provide volume, issue, and page numbers for Ref. 12.

Response: Resolved

Q9 : Please reword text (or caption) of Figs. 19–25, 28 without color words as readers of print will only see black and white figures.

Response: Resolved

DOI : 10.1115/1.4047451

Research Paper

CFD and VIV

[Q1] An Experimental and Numerical Study of Added Mass and Damping for Side-by-Side Plates in Oscillating Flow [Q2]

Frøydis Solaas¹

SINTEF Ocean AS, Energy and Transport, NO-7465, Trondheim, Norway e-mail: froydis.solaas@sintef.no

Fredrik Mentzoni

Department of Marine Technology, Norwegian University of Science and Technology, NO-7491, Trondheim, Norway e-mail: fredrik.mentzoni@ntnu.no

Mia Abrahamsen-Prsic

Department of Marine Technology, Norwegian University of Science and Technology, NO-7491, Trondheim, Norway e-mail: mia.prsic@ntnu.no

Trygve Kristiansen

Department of Marine Technology, Norwegian University of Science and Technology, NO-7491, Trondheim, Norway e-mail: trygve.kristiansen@ntnu.no

¹ Corresponding author.

Contributed by the Ocean, Offshore, and Arctic Engineering Division of ASME for publication in the JOURNAL OF OFFSHORE MECHANICS AND ARCTIC ENGINEERING. Manuscript received June 27, 2019; final manuscript received May 22, 2020; published online . Assoc. Editor: Francisco J. Huera-Huarte.

History : received : 2019-06-27 revised : 2020-05-22 accepted : 2020-05-22 2020-06-09

ABSTRACT

Forced harmonic oscillations of nine configurations consisting of horizontal side-by-side plate elements are performed experimentally and numerically. The configurations are oscillated in vertical direction and represent generalized mudmats of subsea structures. The tests are performed for Keulegan–Carpenter (KC) numbers relevant for force estimation during lifting operations. Hydrodynamic added mass and damping coefficients are presented. The coefficients are found to be amplitude dependent for all tested configurations. The interaction effects between the plates increase with increasing amplitude and decreasing distance between the plates. For small oscillation amplitudes, compared with the gap between the plates, the plates behave approximately like individual plates. A study of the relation between the damping force and the added mass force for the tested structures illustrates the importance of applying representative damping coefficients in numerical analysis of marine operations.

Numerical results are obtained using a potential flow solver (BEM) and a viscous flow solver (CFD). Low-KC added mass coefficients predicted with the BEM are in accordance with the experiments. There is acceptable agreement between the CFD and the experiments. Best agreement is obtained for small KC numbers. As the KC numbers increase, the differences are, in general, larger. This is possibly due to the CFD being based on the two-dimensional laminar flow.

KEYWORDS

- Subsea structures
- dynamics of structures Side-by-side plates
- hydrodynamics Added mass and damping [Q3]

Introduction

Numerical modeling and simulations of the deployment of complex subsea structures are commonly used to obtain the limiting sea-state for the installation operation and to assess forces in the lifting equipment and on the structure to be installed. Together with the vessel capacity, the limiting sea-state will, in many cases, be dependent on the hydrodynamic data used for the structure in the simulations. Overestimation of the expected hydrodynamic loads during the installation may lead to a too low limiting sea state with unnecessary waiting for acceptable weather, or the choice of an oversized vessel. On the other hand, underestimation may lead to an unsafe operation and risk for injury to personnel and damage or loss of equipment. A realistic estimate of the coefficients for the structure in question will therefore have a direct influence on the cost and safety of the installation.

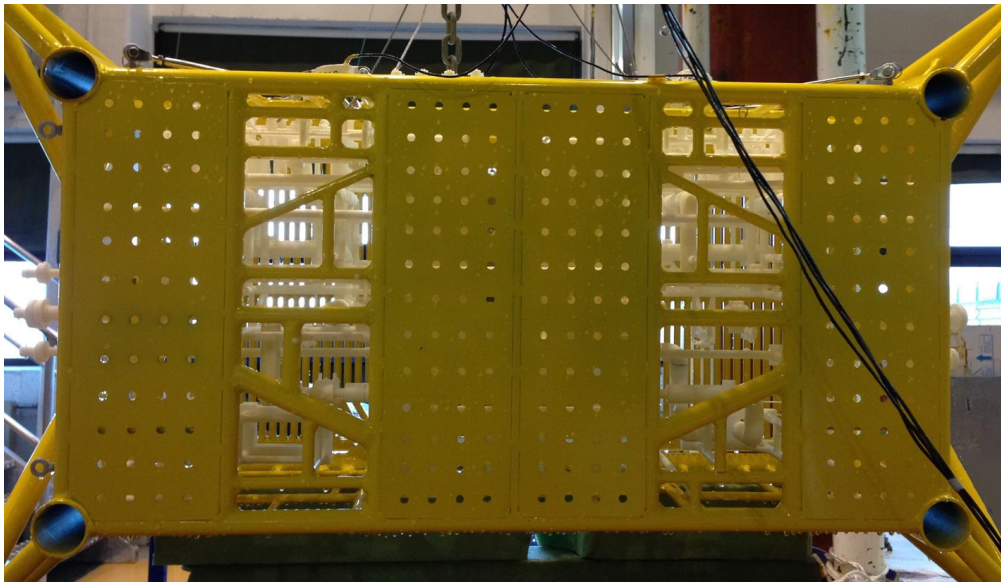
Hydrodynamic added mass and damping for a structure may be obtained by model tests or computational fluid dynamics (CFD) calculations of the complete structure in question. In many cases, the model test data for the structure to be installed are not available and are costly to perform. The same is the case with CFD simulations. The structures often consist of numerous elements, some of them perforated and some solid, which demands detailed numerical models with a large resolution of the mesh in three dimensions and considerable computation time. Therefore, a realistic solution for the project engineer is often to perform a manual estimation of added mass and damping for the structure based on the published data for similar structures and structure parts.

Added mass and damping coefficients for simple structures like plates and cylinders are given in several textbooks including those by Sarpkaya and Isaacson [1], Sumer and Fredsøe [2], Zdravkovich [3], and in the recommended practice for modeling and analysis of marine operations, DNVGL-RP-N103 [4].

When estimating hydrodynamic coefficients for a complete structure based on data for individual structure members, the question about interaction effects between the different members arises. Is it correct to estimate the coefficients as a sum of the contributions for the different parts, or will shielding and interaction dominate the forces? Another topic to consider in the estimation is the amplitude dependency of the coefficients.

The mudmat part of a subsea structure often consists of two or more side-by-side plates with small perforation ratio, side-by-side with and gap(s) between them to accommodate for the subsea equipment. An example of a typical mudmat structure is shown in [Q4] Fig. 1. Several studies are performed and published on single plates with various perforation, like the studies presented by Mentzoni et al. [6], An and Faltinsen [7] and Molin [8]. However, there is a lack of published data for side-by-side plates.

Fig. 1 Model of a typical mudmat structure [5]



To obtain knowledge about the hydrodynamic forces on and interaction of the side-by-side plates, an experimental study is performed. Nine configurations, consisting of one, two, three, and four horizontal solid plates with gap(s) between them, are oscillated harmonically in the vertical direction in a glass wall flume. Solid plates are chosen because it is assumed that they will be representative for mudmat plates with perforation less than around 5%, as suggested by DNV GL [4], Sec. 4.6.4. In addition, hydrodynamic coefficients for the tested configurations are calculated by use of an in-house CFD code and a potential theory boundary element code (BEM), and compared with the model test results.

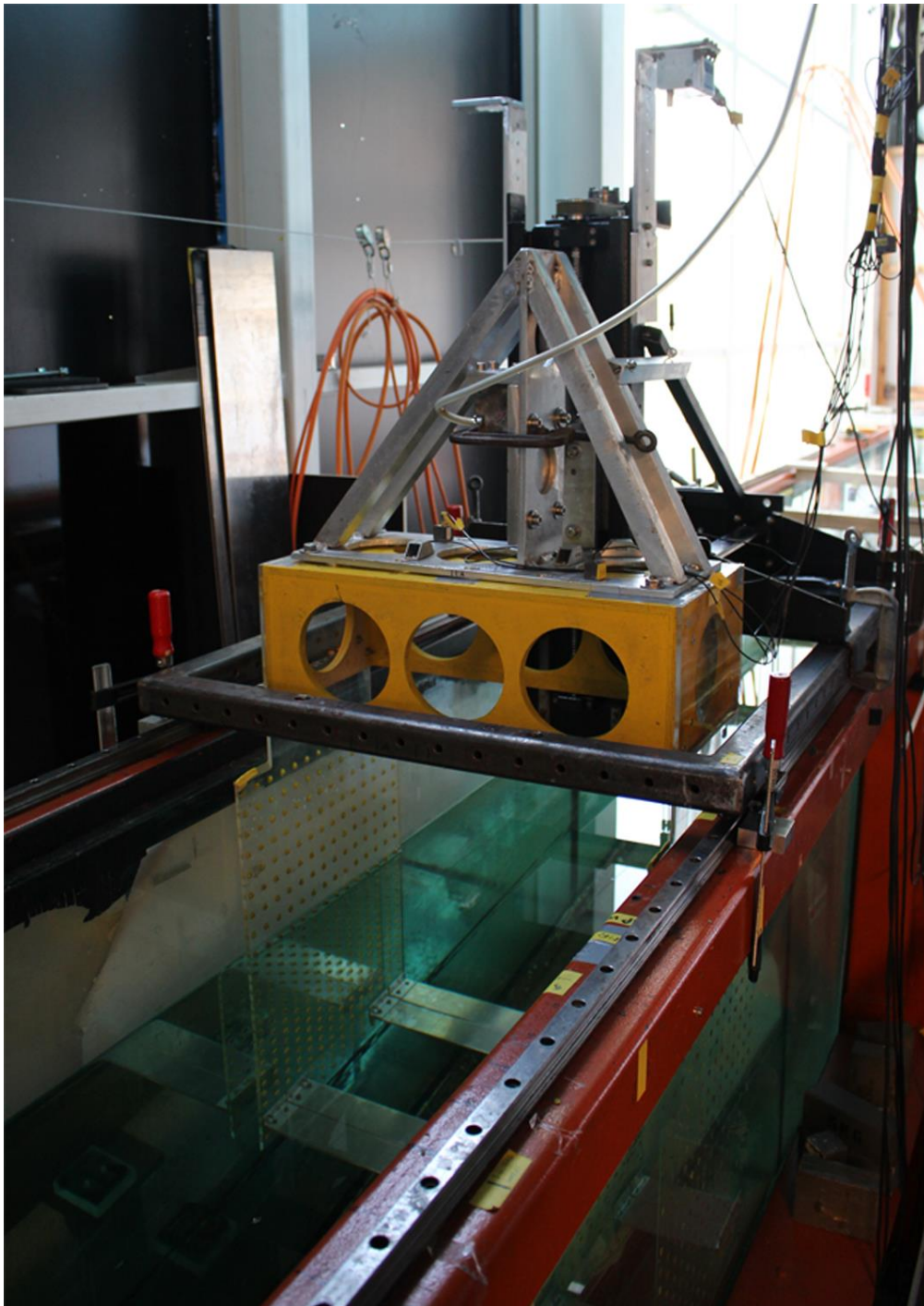
The work is performed as a collaboration between the Norwegian University of Science and Technology (NTNU) in Trondheim and SINTEF Ocean, and is a part of the SFI Marine Operations MOVE, started in 2015 by NTNU, MARINTEK, and SINTEF. The presented experiments are a part of a larger study to provide the project engineers with more knowledge about how to estimate hydrodynamic coefficients, both for use in installation analysis and in onboard decision tools. To provide the project engineers with coefficients for different structures and structure parts is one of the topics in the project. Another is to study if and when coefficients for complete structures may be estimated as a sum of the coefficients of the different parts and when interaction effects have to be taken into account.

Experimental Setup

The hydrodynamic coefficients for the horizontal side-by-side plate models are estimated by use of forced oscillation tests, where the model is oscillated harmonically in the vertical direction. The tests are performed in a wave flume. The tank is 13.5 m long and 0.60 m wide with parabolic beaches placed on both ends of the tank to avoid wave reflections. The test rig is placed in the middle of the tank, 6.5 m from each side. The water depth is 1.0 m in all tests.

The oscillating test rig consists of two acrylic glass plates where the model is mounted between the plates. The acrylic glass plates are used to avoid the end effects and give a near two-dimensional setup. The plates are connected to a steel frame with an actuator on the top (Fig. 2). The distance between the acrylic plates and the glass walls of the tank is approximately 9 mm. The actuator moves in the vertical direction along a rail and is driven by an electrical motor through a belt drive. Forced sinusoidal oscillation sequences are used as input signal for the electrical motor. The signal is read by the actuator at a sample rate of 50 Hz. The force on the entire rig is measured by a 6 kN force transducer located at the intersection between the model rig and the actuator. The motion of the rig is monitored by six accelerometers, while the free-surface elevation is measured by six wave probes at three different distances between the rig and the beaches. All measurements are recorded at a sample rate of 200 Hz with Butterworth filtering at 20 Hz.

Fig. 2 Test tank and model rig with actuator



The test sequences consist of harmonically oscillating signals, with prescribed amplitude and period of oscillation. Each sequence consists of 20 periods of oscillations. The first 5 and the last 5 are used to ramp the signal gradually from zero to the prescribed amplitude of motion and down to zero again.

A more detailed description of the test facility, rig, measurement method, and discussions about the accuracy of the experiments are given in Ref. [6].

Hydrodynamic Coefficients

The hydrodynamic added mass and damping coefficients from the model tests are calculated from the measured vertical force and acceleration. The force measured without any model in the rig is subtracted time-step by time-step in order to obtain the net force on the tested configuration of plates. Assuming a linear damping model, the force F may be written as

$$F=(M+A)\ddot{z}+B\dot{z} \quad (1)$$

where M is the structure mass in air, A is the hydrodynamic mass in the vertical direction and B the damping. The total mass can then be found as the part of the force in phase with the acceleration, \ddot{z} , and the damping as the part in phase with the velocity, \dot{z} . Added mass is then obtained by subtracting the mass of the model in air from the total mass. Since the motions are harmonically varying, the coefficients are obtained by Fourier averaging,

$$(M+A) \int_{-sT}^s \ddot{z} dt + 0 = \int_{-sT}^s F \ddot{z} dt \quad (2)$$

$$0 + B \int_{-sT}^s \ddot{z} dt + 0 = \int_{-sT}^s F \ddot{z} dt \quad (3)$$



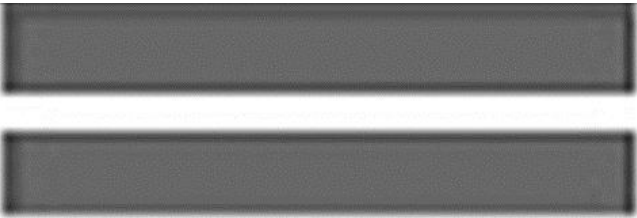
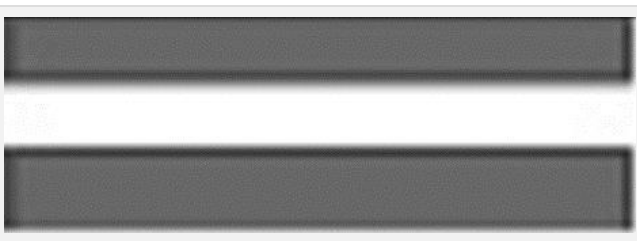
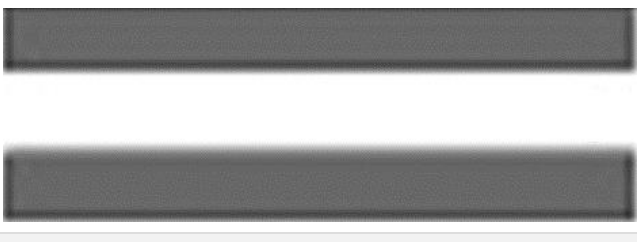
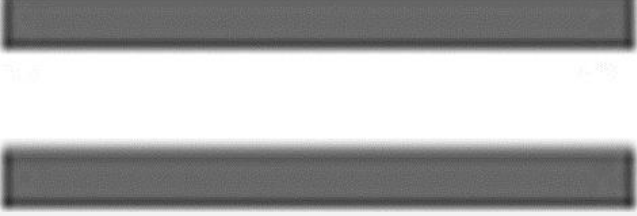
where the integrations are performed over an integer number, n , periods of oscillations, T . The measured force and acceleration are band-pass filtered around the basic harmonic of the oscillation. The presented results are based on the mean of the coefficients obtained from eight of the ten steady-state forcing periods, avoiding the first and last forcing periods as well as the ramp-in and ramp-out. The standard deviations, based on the eight oscillation cycles, are plotted as bars in some of the result figures to visualize the variations of the coefficients between the individual cycles.

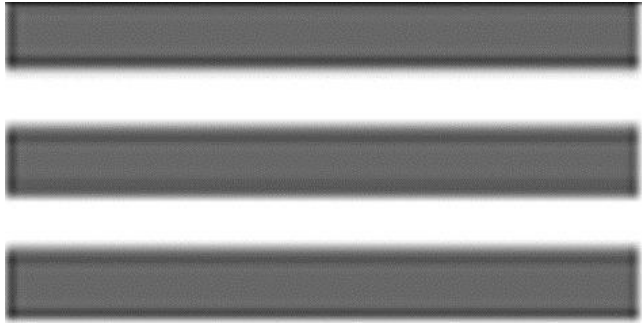
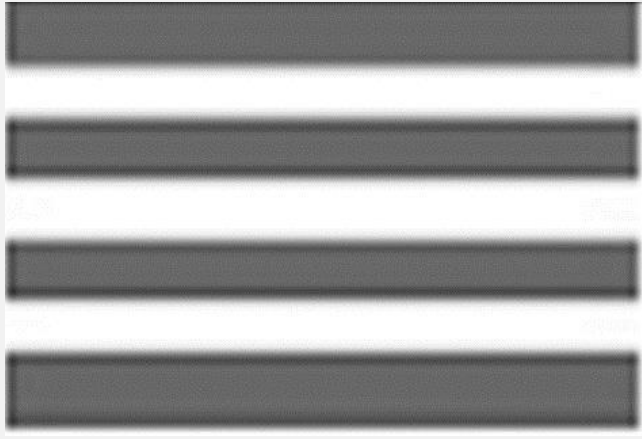
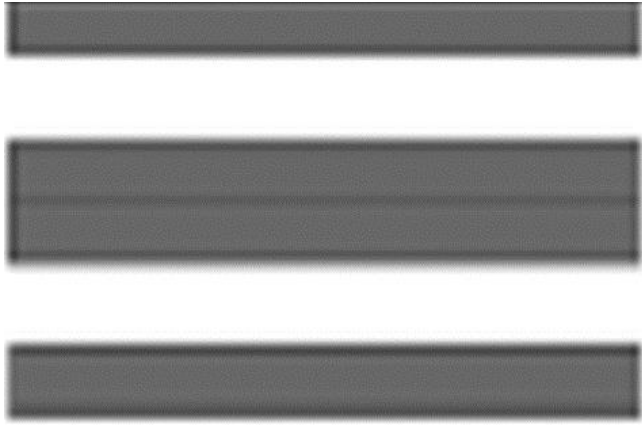
In some figures, dimensionless coefficients are presented. The coefficients are made nondimensional by the infinite fluid added mass for a two-dimensional solid flat plate as predicted by potential flow theory

$$A_0 = \rho \pi \frac{D^2}{4} L \quad (4)$$

The total width, D , for the different configurations are given in Table 1. In all experiments, $L = 0.57$ m.

Table 1 Plate configurations tested

Model	N	D (m)	Gap (m)	Configuration	A_0 (kg)	Perforation ratio $p = 1 - N d/D$	Amplitudes Z (mm)	KC	BEM A/A_0
1P0	1	0.06	–		1.61	0	17–48	1.7–5.0	1.107
2P0	2	0.12	0		6.45	0	17–97	0.9–5.0	1.066
2P20	2	0.15	0.03		10.07	0.20	17–60	0.7–2.5	0.389
2P33	2	0.18	0.06		14.50	0.33	17–72	0.6–2.5	0.258
2P43	2	0.21	0.09		19.74	0.43	17–83	0.5–2.5	0.186
2P50	2	0.24	0.12		25.79	0.50	17–95	0.4–2.5	0.141

3P40	3	0.30	2 × 0.06		40.29	0.40	17–95	0.36– 2.0	0.142
4P43A	4	0.42	3 × 0.06		78.97	0.43	17–120	0.25– 1.8	0.098
4P43B	4	0.42	2 × 0.09		78.97	0.43	17–120	0.25– 1.8	0.139

Note: N is the number of plate elements, D is the total width of the model, d is the width of one plate, and A_0 is the corresponding potential added mass of a solid plate.

The results are presented as a function of the Keulegan–Carpenter (KC) number

$$KC = \frac{WT}{D} \quad (5)$$

with W being the velocity amplitude. For harmonic motions, this can be written

$$KC = 2\pi \frac{Z}{D} \quad (6)$$

with Z being the amplitude of motion. The damping coefficients are made nondimensional by A_0 times the frequency of oscillations, $\omega = 2\pi/T$.

Tested Plate Configurations

Nine different plate configurations are tested. The configurations consist of one to four solid steel plates, all with length $L = 0.57$ m, width $d = 0.06$ m, and plate thickness $t = 4$ mm, as shown in Fig. 3. This thickness is chosen to ensure that the plates have a large enough stiffness to avoid vibrations of the plates during the tests. With a width-to-thickness relation of $60/4 = 15$, the steel plates may be considered as relatively thin. The initial distance from the center of the model to the free surface and to the bottom is 0.5 m.

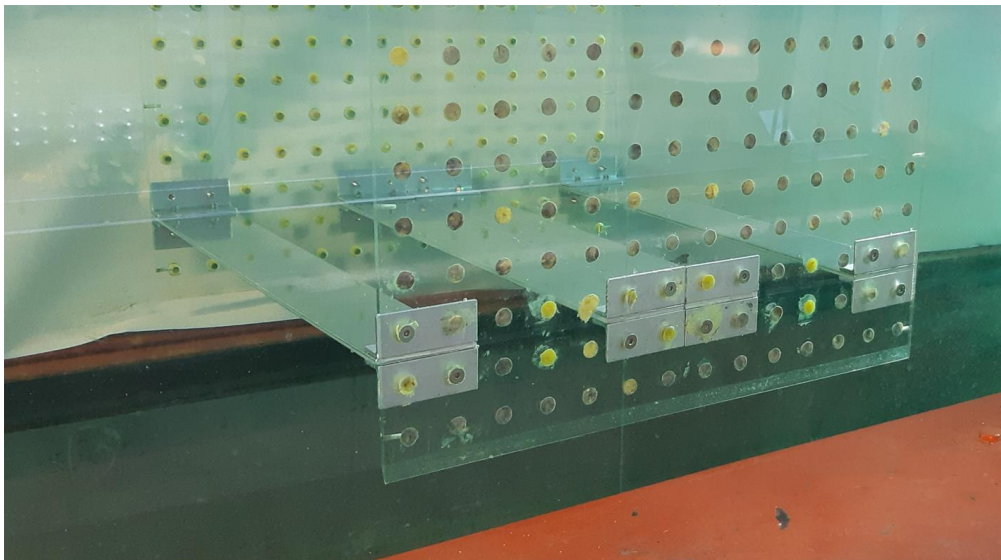
Fig. 3 Side- and top views of steel plate model



Table 1 gives an overview over the tested of plate configurations tested. The naming convention is following: The first number refers to the number of plates in the model setup and the last number to the perforation ratio. The perforation ratio is calculated as the total open area of the model divided by the total outer area.

Figure 4 shows the model 4P43B in the tank, seen from the side of the tank. The yellow dots are holes in the acrylic side plate where the models may be connected with screws. The holes are sealed with yellow putty when not in use to prevent flow through the side plates.

Fig. 4 Side view of model 4P43B mounted between the acrylic glass plates in the test tank



All models are tested with a period of oscillation $T = 2$ s. In addition, the 1P0 and 4P43B models are tested with $T = 1$ s, 1.25 s, 1.5 s, and 1.75 s. The amplitude of motion range for all of the different models is given in Table 1. If setup 4P43A is used as reference and assumed to be a generalized representation of the mudmat on a subsea structure with width 8.4 m, $T = 2$ s corresponds to a full-scale period of oscillation around 9 s and amplitudes correspond to between 0.3 and 2.4 m. Realistic KC number for an installation operation will be up to around $KC = 2$, as chosen in this study. Since KC number varies with structure dimension D , different amplitude ranges are used for the different configurations.

Computational Fluid Dynamics Method

A two-dimensional CFD method considering laminar flow is used in the present study. The code is a numerical Navier–Stokes solver, based on the fractional-step method, as that by Chorin [9]. The governing equations of motions are solved on a Cartesian grid, using a staggered grid approach. The implementation allows for variable grid cell sizes through the domain, with a fine, high-resolution, region close to the structures, and increasing cell sizes toward the boundaries of the computational domain.

First-order upwind schemes are used for the advection terms of the Navier–Stokes equations. Second-order central schemes are used for the other spatial differentials. Time-stepping is performed using the implicit Euler scheme with a step size

$$\Delta t = \min \left(0.005T, 0.2 \frac{\min(\Delta x, \Delta z)}{W} \right) \quad (7)$$

where $\min(\Delta x, \Delta y)$ is the length of the smallest cell size and T is the period of oscillation, set equal to that of the experimental investigation, $T = 2$ s. Furthermore, the density and kinematic viscosity of the simulations are set to match the conditions in the experimental investigations. More details on the numerical implementation are provided in the study by Mentzoni and Kristiansen [10], which also contain several sensitivity studies.

The nine experimentally tested plate configurations are numerically simulated. The domain size and grid refinement are studied in detail in Ref. [10] and are chosen accordingly in the present study. Details are presented in Table 2. The computational domains have lengths of equal size in both dimensions, approximately 13–17 times the total widths of the configurations. Consequently, the simulations are performed with approximately infinite fluid conditions.

Table 2 Discretization of CFD models

Model	D	D/Δ	l/D	Cell count
1P0	0.06	30	13.6	3252
2P0	0.12	60	13.7	7196
2P20	0.15	75	16.0	9610
2P33	0.18	90	13.6	12,516
2P43	0.21	105	16.7	16,890
2P50	0.24	120	14.7	18,060
3P40	0.30	150	14.7	30,500
4P43A	0.42	210	14.4	52,260
4P43B	0.42	210	14.3	52,260

Note: D is the plate width; D/Δ is the width-to-cell size in the fine grid region close to the plate; l/D is the domain size to plate width, and Cell count is the total number of grid cells in the domain.

Hydrodynamic coefficients are calculated based on the total force on the configurations in the simulations. The water is forced to oscillate harmonically in the entire domain, such that the configurations experience an ambient, sinusoidally oscillating flow. The Froude–Krylov force is subtracted, in order to have comparable coefficients to the experimental investigations, where the configurations themselves, not the surrounding water, are forced to oscillate.

In previous investigations using the present CFD to simulate perforated plates in oscillating flow [10] and [11], the calculated coefficients were found to yield minor standard deviations between successive cycles of oscillation within each simulation. Consequently, using a small number of simulated periods was previously found sufficient, typically 6–10. This is not the case for all side-by-side plate configurations in the present study. A larger range of oscillation periods, 30, are therefore used in the present study, and both the mean of and the standard deviations between the coefficients of the different oscillation periods are presented. The ten first oscillation periods are ignored when performing the calculations.

Source Method

Added mass coefficients in the low-KC limit are calculated with a two-dimensional boundary element method (BEM). The results are presented in Table 1.

In the present BEM, sources with constant strengths are distributed along discretized configurations with equal dimensions (width \times thickness) as those experimentally investigated. All configurations have finite thickness. Hence, a source method is applicable. The code has been verified against analytical solutions for the added mass of simpler structures. Based on tests of the numerical convergence, 100 elements are used to discretize each plate element (60 mm \times 4 mm). Consequently, the total number of elements in the configurations are 100 (1P0), 200 (2P0, 2P20, 2P33, 2P43, 2P50), 300 (3P40), and 400 (4P43A, 4P43B). Configuration 2P0 is modeled as one plate with dimensions 120 mm \times 4 mm using 200 elements.

As seen in Table 1, $A/A_0 = 1.107$ for 1P0 and 1.066 for 2P0. For an infinite thin plate, the values should be 1.000. The 2P0 model has a D/t relation equal to 30. To check the BEM solution, simulations with $D/t = 3000$ are performed. For 200 elements $A/A_0 = 1.010$ and 2000 elements 1.001.

Results

In general, there is a good or satisfactory agreement between the model test results and the CFD calculations for small KC numbers. For the larger KC numbers, the difference is larger and dependent on the plate setup. Generally, this may be explained with different flow conditions between the experiments and the CFD. The numerical solution is based on two-dimensional, laminar flow. Even though the experimental setup is quasi two dimensional, the nature of the flow and the finite spanwise length allow three-dimensional flow variations along the model.

Solid Plate Configurations

Results for solid plates, 1P0 and 2P0, are presented in Figs. 5 and 6, for added mass and damping, respectively.

Fig. 5 Added mass coefficients as function of KC number for solid plates with width 60 mm (1P0) and 120 mm (2P0)

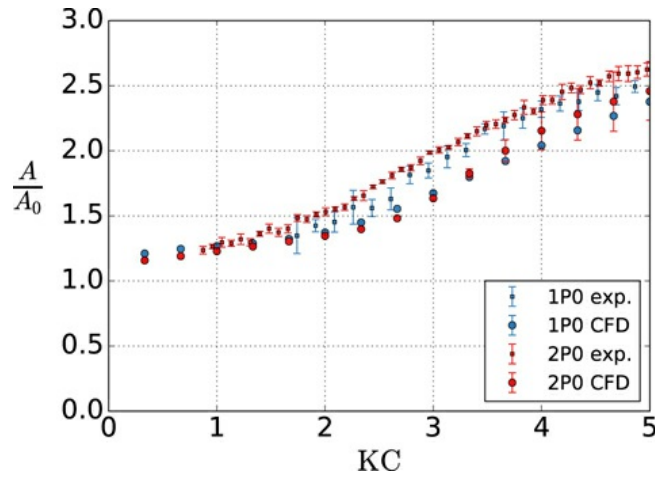
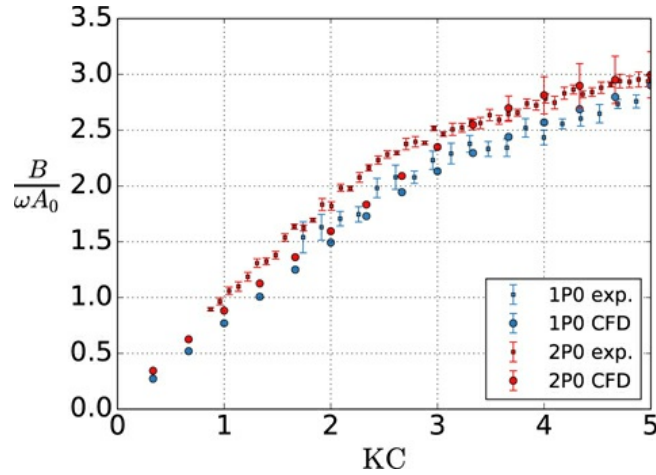


Fig. 6 Damping coefficients as function of KC number for solid plates with width 60 mm (1P0) and 120 mm (2P0)



The obtained added mass coefficients increase with increasing KC number. The values are somewhat higher in the experiments than in the CFD, dependent on the KC number. For $KC = 1$, the difference is 4% percent. For KC around 3, the difference is 10% percent for 1P0 and 20% percent for 2P0.

When KC approaches 0, both the experiments and the CFD approach values close to the values obtained with the BEM solver, as given in Table 1. These values are larger than 1.0, due to the finite thickness of the plate models. The added mass coefficient is up to 12% lower for 1P0 than for 2P0 and the standard deviation for the 1P0 model test results is also larger than for the 2P0 model. Possible reasons for the differences may be three-dimensionality in the flow around the plates and due to the different t/D ratios relations for the two setups, where $D/t = 30$ for 2P0 and 15 for 1P0. Tian et al. [12] have investigated the effect of different plate thickness for circular discs. Their results show a decrease in both added mass and damping for increasing thickness relative to the diameter of the disc, which is in accordance with our results.

Another reason may be that the flow in the experiments is not laminar, as in the CFD code. The Reynolds number is given by

$$Re = \frac{WD}{\nu} \quad (8)$$

where W is the vertical velocity magnitude, D the characteristic length (in our case, set equal to the width of the configuration) and ν the kinematic viscosity, which is equal to $9.55 \times 10^{-7} \text{ m}^2/\text{s}$ for water at a temperature of 22 °C. For an amplitude of oscillation equal to 16 mm and period 2 s, the velocity is $W = 0.05 \text{ m/s}$. With $D = 0.06 \text{ m}$, this gives a Reynolds number $Re = 3140$. For amplitude 48 mm, $W = 0.15 \text{ m/s}$ and $Re = 9420$. The wake flow will then be turbulent.

For the damping, the agreement between the model tests and CFD is better for all the KC numbers tested. The 1P0 model gives smaller damping values than the 2P0 model.

There is a lack of published model test results for setups which corresponds to the present nearly two-dimensional setup with no flow around the short edges. Tian et al. [12] show results for some rectangular plates with different length-to-breadth ratios. The B7 model in Ref. [12] has a length-to-breadth ratio relation equal to 4, which is the one closest to the 2P0 model with a length-to-breadth ratio relation equal to 4.75. According to Sarpkaya and Isaacson [1], a length-to-breadth ratio relation of 4 gives an added mass equal to 0.872 times the value for a two-dimensional plate, A_0 , as given by Eq. (4). This means that the results for the B7 model in Ref. [12] and the 2P0 model cannot be compared without considerations.

Tian et al. [12] use a characteristic dimension of the model equal to the diameter of a circular disc with the same area as that of the rectangular plate and makes the results nondimensional by the theoretical ideal fluid added mass for the disc. If the breadth of the plate is used instead and the results made nondimensional by $0.872 A_0$, it is observed that there is quite good agreement in the added mass for KC less than 2.4 and damping for KC less than 1.1, while both added mass and damping from [12] are smaller for larger KC numbers.

Two-Plate Configurations

Results for the two side-by-side plates configurations with varying gap, 2P20, 2P33, 2P43, and 2P50 are shown in Figs. 7 and 8.

Fig. 7 Added mass coefficients as function of KC number for two side-by-side plates with different distances between them

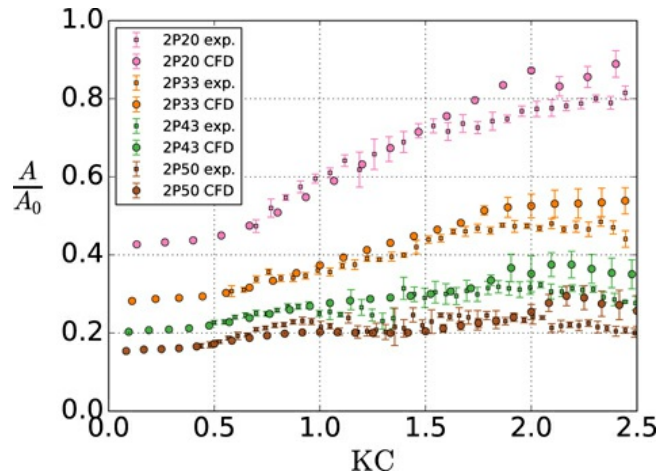
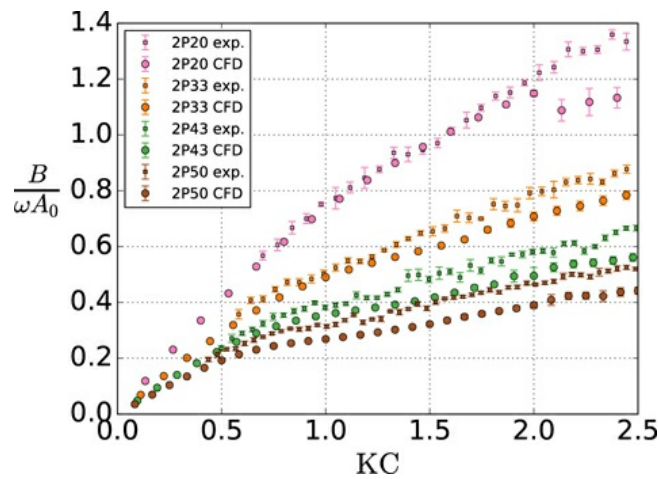


Fig. 8 Damping mass coefficients as function of KC number for two side-by-side plates with different distances between them



Generally, the added mass decreases with increasing gap between the plates. Both added mass and damping increase with increasing amplitude of oscillation. An interesting observation is that for the cases with the largest gaps, 2P43 and 2P50, there is a dip in the added mass values for KC numbers between 1.0 and 1.5. Another interesting observation, most clearly observed in the experimental results, is that for large KC numbers, the added mass curves show a tendency to flatten out and decrease.

If the results for added mass are extrapolated toward $KC = 0$, the added mass value will end somewhat above the values obtained by the BEM solution, cf. Table 1.

Three-Plate Configuration

Results for three side-by-side plates with the gap equal to the plate width are shown in Figs. 9 and 10. For KC numbers less than 1.0, there is a good agreement in the added mass between experiments and CFD, with a difference less than 7% percent. It is interesting to notice that a similar dip in the added mass values in the experiments for KC numbers between 1.0 and 1.5, as observed for the two-plate configurations, is seen here as well.

Fig. 9 Added mass coefficients as function of KC number for three side-by-side plates with the gap equal to the plate width (3P40)

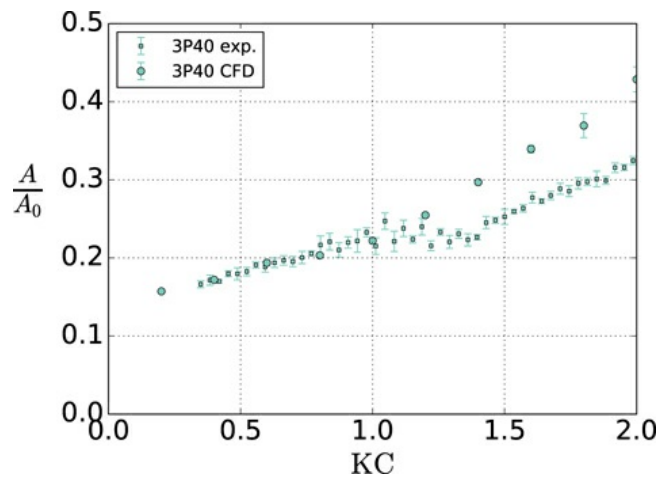
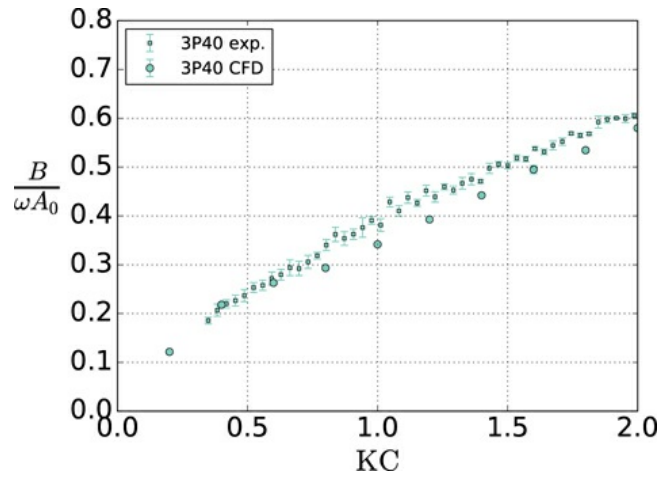


Fig. 10 Damping coefficients as function of KC number for three side-by-side plates with the gap equal to the plate width (3P40)



When KC approaches zero, the added mass coefficient goes toward a value close to the value obtained by the BEM solution, which is 0.142.

Except for the smallest KC numbers, the model test results give larger damping than the CFD.

Four-Plate Configurations

Results for the four-plate configurations, 4P43A and 4P43B, are presented in Figs. 11 and 12.

Fig. 11 Added mass coefficients as function of KC number for the four-plate configurations 4P43A and 4P43B

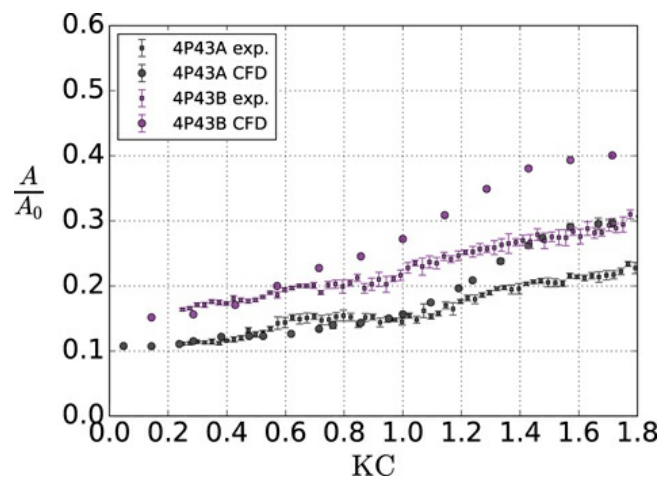
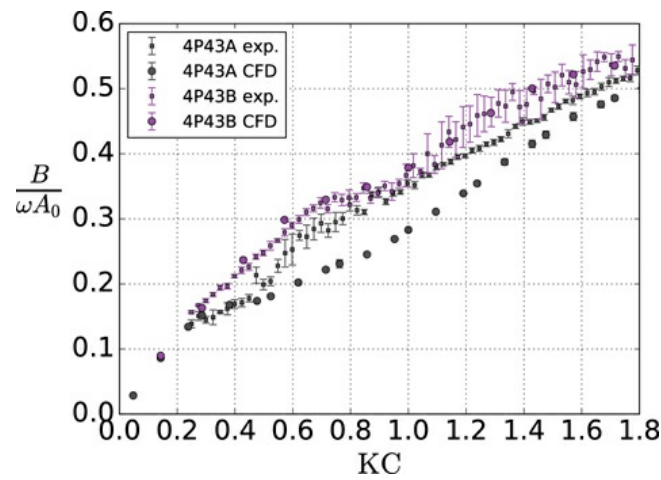


Fig. 12 Damping coefficients as function of KC number for the four-plate configurations 4P43A and 4P43B



Considering For added mass, there is a good agreement between the experiments and the CFD for KC numbers smaller than 1.1 for the 4P43A configuration, and for KC numbers less than 0.6 for the 4P43B configuration. For larger KC numbers, the numerical simulations predict larger added mass values than the experiments.

When KC approaches zero, the added mass coefficient for 4P43A goes toward a value just above 0.1. The infinite fluid potential theory BEM code gives a value of 0.0982 for the 4P43A setup modeled with 400 elements. If the four plates are regarded as four superposed individual plates with no interaction, the infinite fluid solution for one plate in Eq. (4) gives $N d^2/D^2 = 0.082$. Hence, there is a 20% increase in the added mass coefficient due to potential flow hydrodynamic interaction.

For the 4P43B configuration, the added mass coefficient goes toward a value just below 0.15. The value obtained by the BEM solution is 0.139.

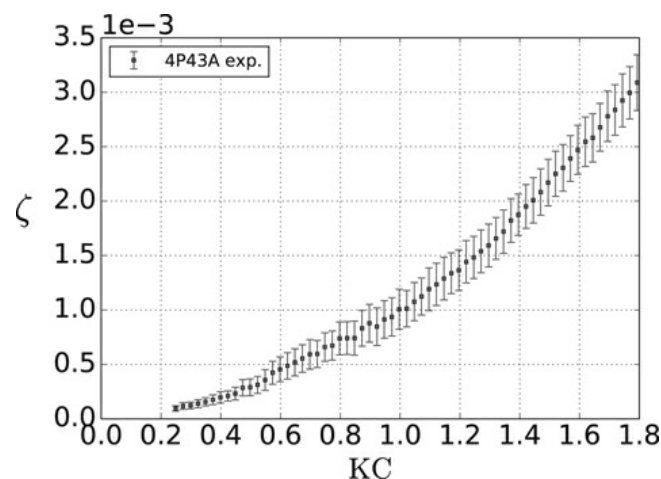
For 4P43A, there is a good agreement in the damping between the experiments and the CFD results for the smallest KC numbers, KC less than around 0.5. For larger KC numbers, the model tests give larger damping than CFD. For 4P43B, there is generally good agreement in the damping for all KC numbers tested.

Wave Generation During Experiments

The water depth in the test flume is 1.0 m, with a mean distance of the model to the free surface equal to 0.5 m. For the largest amplitude of motion in the experiments, the distance to the free surface, when the model is in the upper position, will be 0.38 m. To study if the discrepancy between experiments and CFD for larger amplitudes of motions is due to the wave generation in the test tank, the case with the largest model, 4P43A, is studied.

In Fig. 13, the radiated wave elevation due to oscillations of model 4P43A is presented as a function of the KC number. The wave elevation due to the oscillations of the model is small, around 3 mm for KC = 1.8, which corresponds to an oscillation amplitude of 120 mm. This gives radiation damping of around 2 kg/s, which is small compared to the damping from the model, which is around 130 kg/s at this KC number.

Fig. 13 Measured wave elevation during oscillation of four plates with the gap equal to the plate width

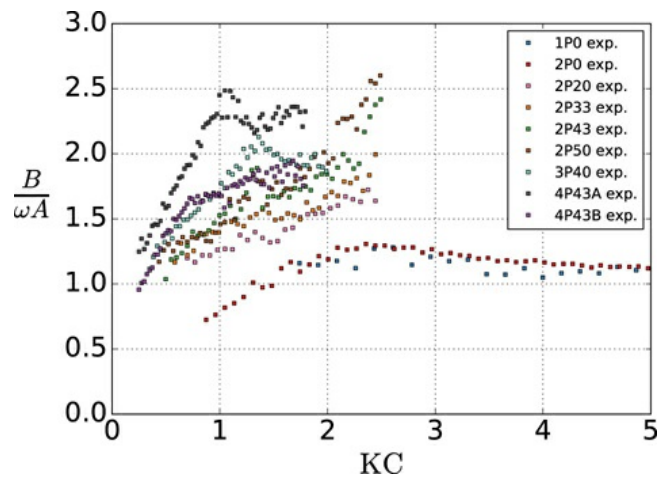


Importance of the Damping Versus the Added Mass

For a structure oscillating harmonically with frequency of oscillation ω , the ratio between the damping force and the added mass force is given by $B/(A\omega)$. When $B/(A\omega) > 1$, the damping force dominates over the added mass force and when $B/(A\omega) < 1$, the added mass will dominate.

The damping-to-added mass ratios for the tested structures are shown in Fig. 14. Damping dominates for all configurations. The damping dominance increases, in general, with increasing KC. This illustrates the importance of using representative damping coefficients in the numerical analysis of marine operations.

Fig. 14 Ratio of the damping force to the added mass force



Importance of the Period of Oscillations

The results for the 1P0 model tested at different periods of oscillations are shown in Figs. 15 and 16, and the results for the 4P43B model in Figs. 17 and 18. For the added mass, the difference between the results for the different periods of oscillations is less than 12% percent, which shows that the period of oscillation has little influence on the added mass for the tested configurations of flat plates. A larger scatter is seen in the damping results for 1P0, where the curves follow the same trend, but with a maximum difference of 30% percent at $KC = 1.7$. For the 4P43B model, the damping curves resemble.

Fig. 15 Added mass coefficients for different periods of oscillations as function of KC number for a solid plate with width 60 mm width (1P0)

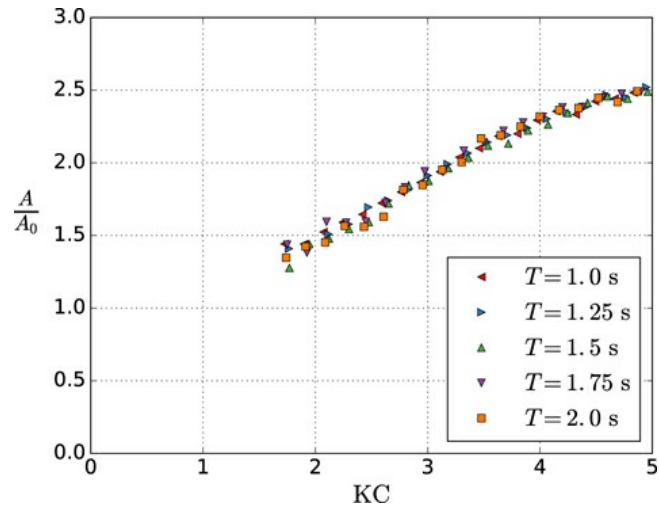


Fig. 16 Damping coefficients for different periods of oscillations as function of KC number for a solid plate with width 60 mm width (1P0)

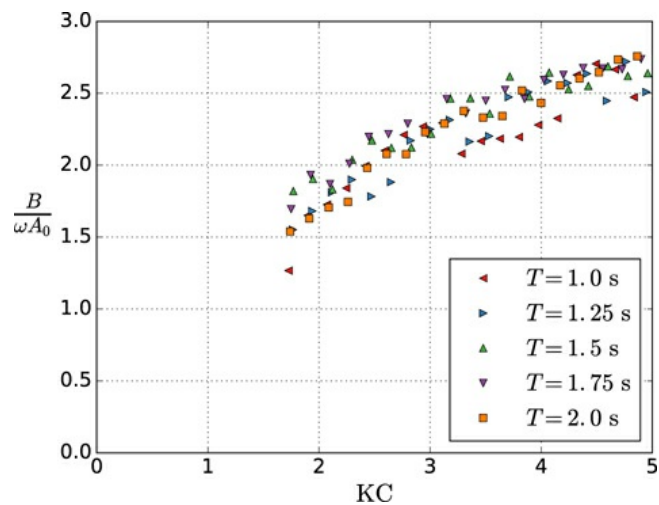


Fig. 17 Added mass coefficients for different periods of oscillations as function of KC number for the four-plate configuration 4P43B

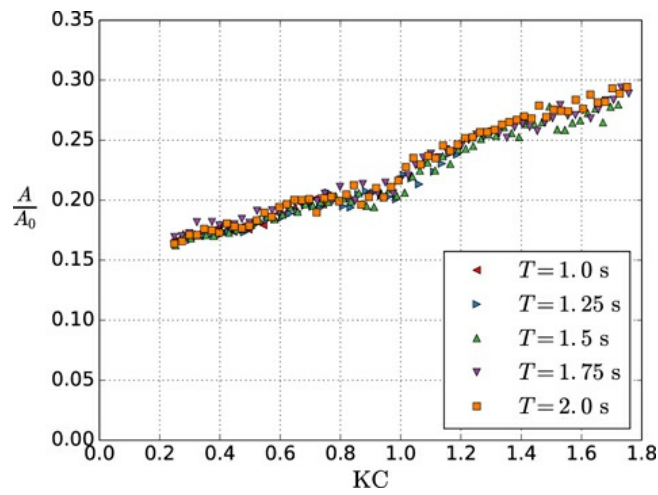
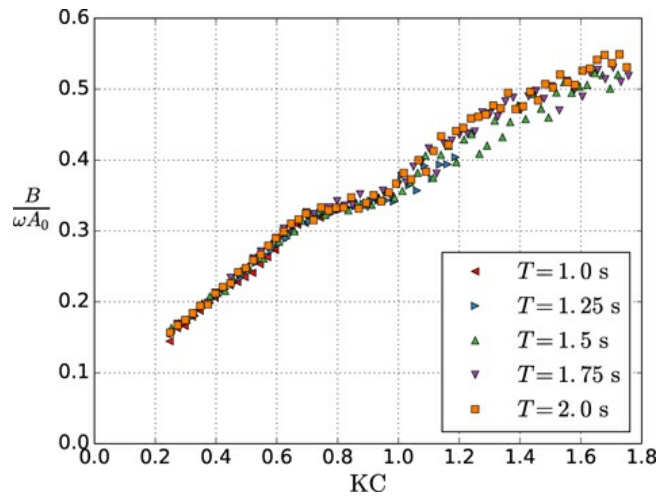


Fig. 18 Damping coefficients for different periods of oscillations as function of KC number for the four-plate configuration 4P43B



Discussion and Estimation of Coefficients

If the data for a complete subsea structure are not available from model tests or CFD, the project engineer has to estimate the added mass and damping for the structure based on the published data for similar structures and structure parts. The estimation is then usually based on available coefficients for individual structure parts that are added together. It may therefore be convenient to discuss the amplitudes of motion and the added mass and damping as dimensioned values.

In Fig. 19, the added mass is shown as a function of the amplitude for the two-plate setups. In addition to the two-plate results, the values obtained by doubling the values for a single plate are shown ($2 \times 1P0$). For small oscillation amplitudes, the added mass and damping values for two times one plate are close to the values for the two plates with larger gaps of 60, 90, and 120 mm. For amplitudes larger than around 30 mm, added mass for one plate $\times 2$ is closer to the values for the two plates with the small gap, 30 mm. For instance, for the amplitude of 45 mm, $2 \times 1P0$ yields about 50% higher added mass than 2P43 and 2P50, but only 3.5% higher than 2P20. The damping, which is shown in Fig. 20, on the other hand, is closest to the values for the plates with the largest gap, 120 mm, for all KC numbers.

Fig. 19 Added mass (kg) as a function of the amplitude of oscillations (cm) for two side-by-side plates with different distances between them. The blue pentagons show twice the values obtained for one single plate.

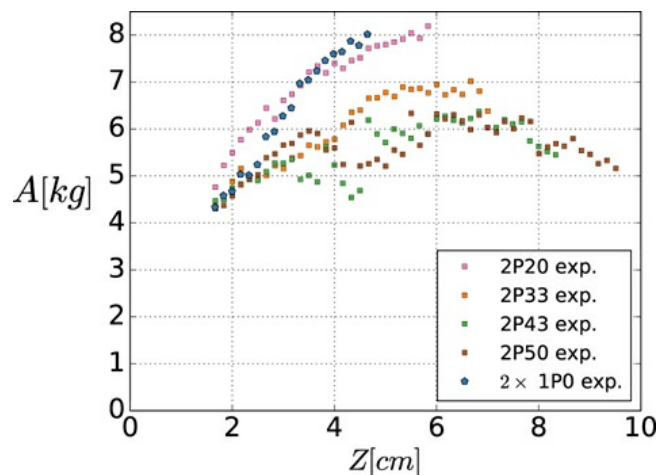
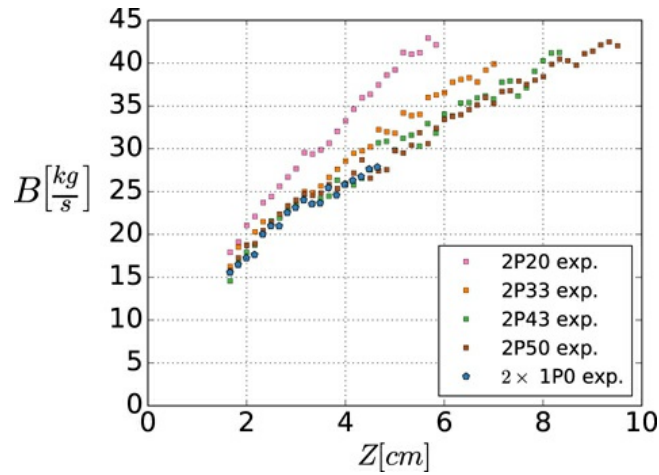


Fig. 20 Damping (kg/s) as a function of the amplitude of oscillations (cm) for two side-by-side plates with different distances between them.

The blue pentagons show twice the values obtained for a single plate [Q9].



The reason that twice the added mass value for a single plate corresponds to the values for gap 60 mm and larger, at small amplitudes of motion, may be that the flow around each of the two plates behaves more like the flow around an individual plate as long as the amplitudes are small. When the amplitudes increase, the flow around the two plates with the gap of 30 mm behaves more like one solid plate, and hence, the estimation based on one plate corresponds better.

In Figs. 21 and 22, a similar analysis is performed for the three-plate configuration. Added mass and damping for 3P40 are compared with three times the values for one plate ($3 \times 1P0$). It is seen that, except for the smallest amplitudes below 2.5 cm, the added mass will be overestimated. The estimation of damping is quite good for amplitudes below around 3.5 cm. For amplitudes above 3.5 cm, the damping is underestimated.

Fig. 21 Added mass (kg) as a function of the amplitude of oscillations (cm) for three side-by-side plates. The blue pentagons show three times the value for a single plate.

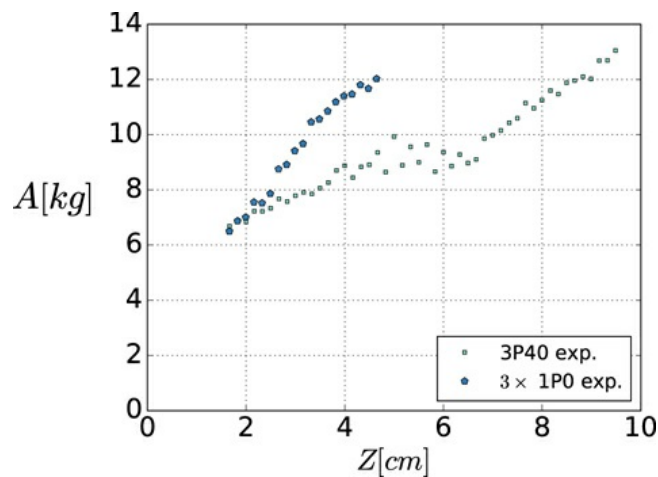
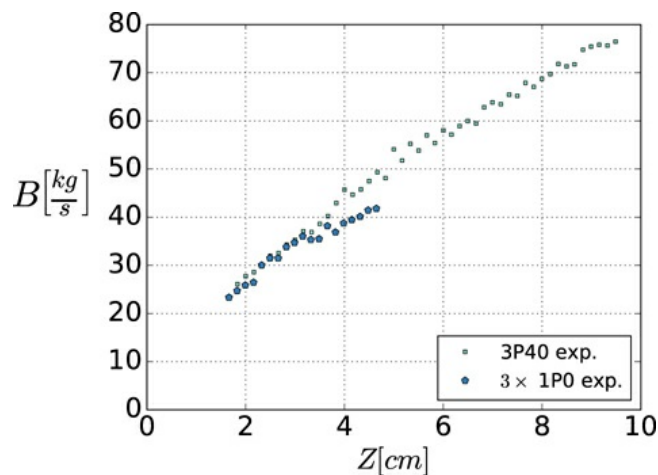


Fig. 22 Damping (kg/s) as a function of the amplitude of oscillations (cm) for three side-by-side plates. The blue pentagons show three times the value for a single plate.



In Figs. 23 and 24, added mass and damping for the four-plate configuration 4P43A are compared with twice the values for 2P33, which has the same gap between the plates, 60 mm, as well as with four times the values for a single plate. The estimations based on a single plate are quite good for the smallest amplitudes. When the amplitude increases, the added mass will be overestimated, and the damping underestimated.

Estimating the added mass and damping based on the results for two plates with the same gap as 4P43A gives better agreement, but still the added mass is overestimated and the damping somewhat underestimated.

Fig. 23 Added mass (kg) as a function of the amplitude of oscillations (cm) for four side-by-side plates. The lower row of pentagons shows twice the values for two plates with the same distance between them, and the top row of blue pentagons four times the value for a single plate.

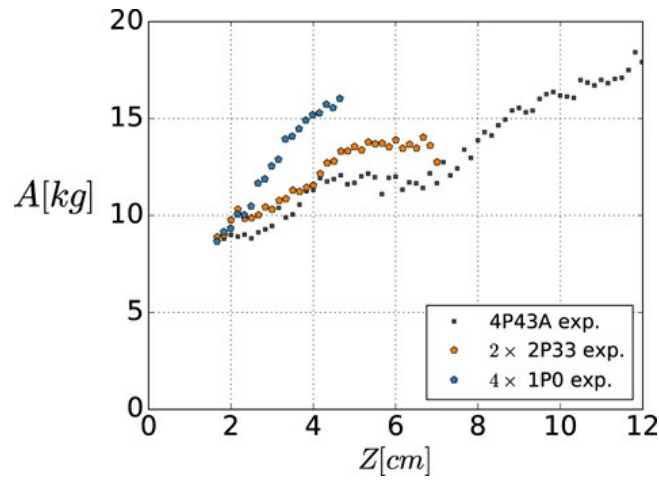


Fig. 24 Damping (kg/s) as a function of the amplitude of oscillations (cm) for four side-by-side plates. The top row of orange pentagons shows twice the values for two plates with the same distance between them, and the bottom row of blue pentagons four times the value for a single plate.

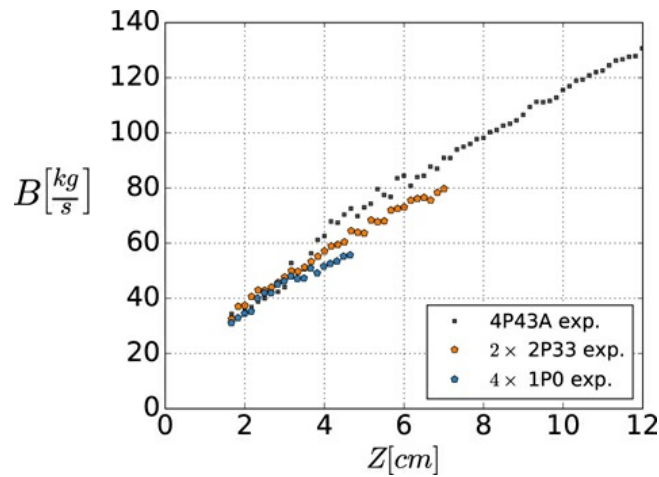
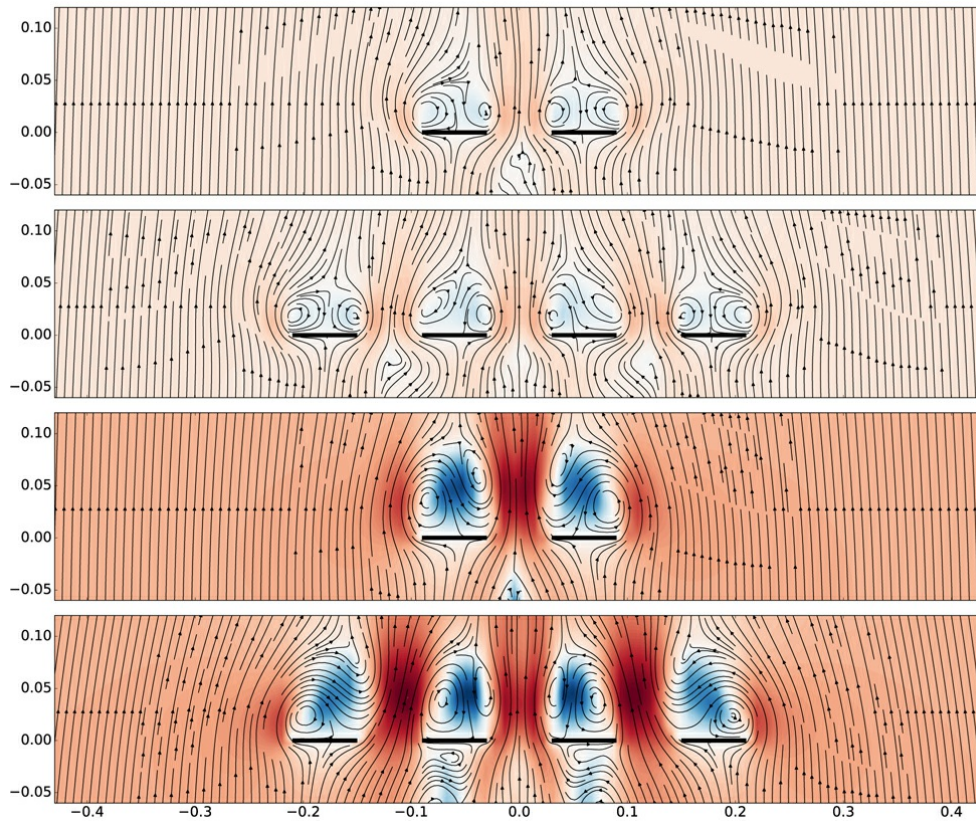


Figure 25 visualizes the flow around two (2P33) and four (4P43A) plates with the same gap between them, as predicted by the CFD. The two upper plots show the streamlines at amplitude 16 mm and the two lower plots the streamlines at amplitude 48 mm. The flow is generally more symmetrical for the low KC case than for the high KC case. The global flow for the models consisting of two and four plates is comparable. The snapshots are taken after 30 periods of oscillations in the CFD simulations, at time instant $30 T + 0.3 T = 60.6$ s.

Fig. 25 Instantaneous streamlines for the flow around two (2P33) and four (4P43A) plates with the same gap between them, from CFD. The two upper plots show the flow at amplitude 16 mm, which corresponds to $KC = 0.555$ and 0.238 for 2P33 and 4P43A, respectively. The two lower plots show the flow at amplitude 48 mm, which corresponds to $KC = 1.667$ and 0.714 , respectively. Contour colormap blue indicates negative vertical velocity and red positive velocity.



An interesting observation is that when plotting the nondimensional results for the models with two gaps 3P40 and 4P43B together, as shown in Figs. 26 and 27, the curves resemble for KC numbers less than 0.8. For larger KC numbers, the difference in added mass is up to 16% percent and in damping up to 15% percent. For KC numbers above 1.5, the curves resemble again. The reason for the similarity between the two models may be that the flow pattern due to two gaps in both models is relatively similar. This assumption is supported by the visualization plots of the flow from the CFD for the two models, shown in Fig. 28.

Fig. 26 Added mass coefficients from model tests as function of KC number for the configurations 3P40 and 4P43B

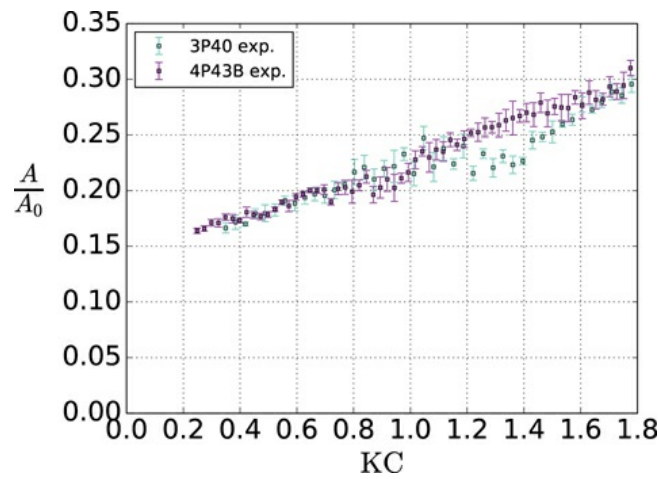


Fig. 27 Damping coefficients from model tests as function of KC number for the configurations 3P40 and 4P43B

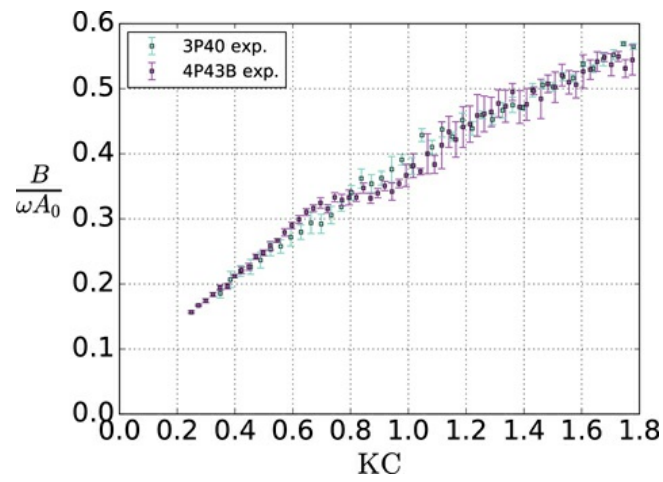
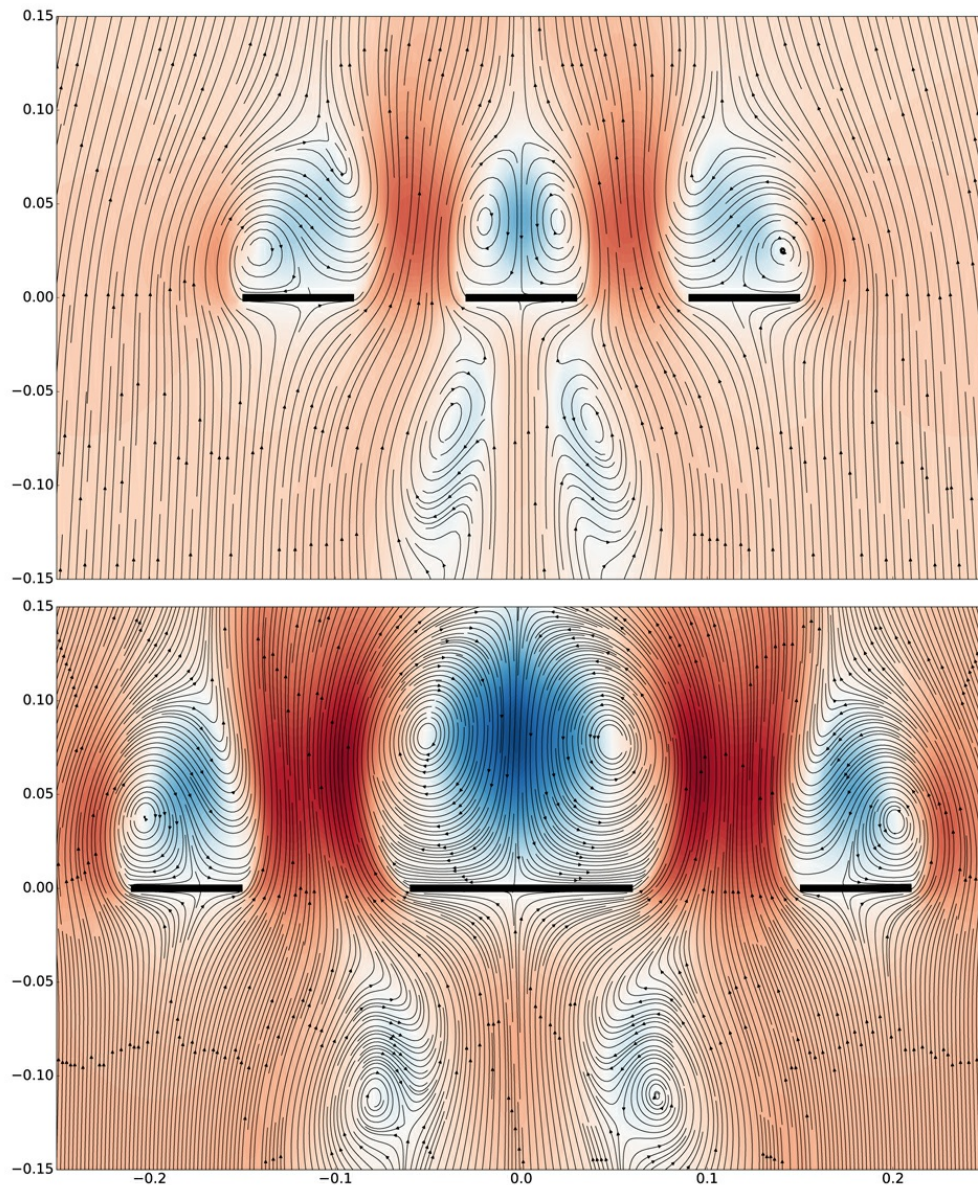


Fig. 28 Instantaneous streamlines of flow around the models with two gaps (3P40 and 4P43B) at $KC = 1.0$ from CFD. Contour colormap blue indicates negative vertical velocity and red positive velocity.



Conclusion

Experimental and numerical results for added mass and damping of horizontal side-by-side plates with varying gap between them were presented. The numerical results, obtained by use of a two-dimensional, laminar CFD code, show good agreement with the experimental results for small and intermediate KC numbers. For larger KC numbers, the experimental and the numerical results diverge. One explanation is that, even if the test setup is nearly two dimensional, the flow around the plates in the model tests may vary along the plates. Another is that the flow in the experiments is not laminar. The wave elevation was measured to be small and excludes wave generation damping as a reason for the difference.

Both added mass and damping were dependent on the amplitude of oscillations. Generally, the added mass was found to increase with increasing

KC number, but a tendency to flatten out and decrease for large KC numbers was observed.

Two main conclusions arise from the results:

1. In general, the damping force was found to dominate over the added mass force. The only exception was for solid plate configurations at small KC numbers. For the configuration with four plates, 4P43A, the damping-to-added mass ratio was 2.2–2.5 for KC numbers between 0.8 and 2. This illustrates the importance of focus on the damping when hydrodynamic coefficients for subsea structures are estimated for use in numerical simulations of the installation operations.
2. When studying the interaction effects between the side-by-side plates in the present configurations, it was seen that the larger the gap between the plates or the smaller the KC number (amplitude of oscillation), the more the side-by-side plates behave like individual plates. When the amplitudes increase or the size of the gap decreases, the interaction effects between the plates become more important.

The present study highlights that the hydrodynamic coefficients for a subsea structure consisting of several parts cannot be estimated as the sum of the coefficients from the individual parts without considerations of the structure type, amplitudes of oscillation, and interaction effects. Future work will include studies of the other key components of subsea modules, like the mudmat, roof, and equipment inside the module. They will be studied both as individual elements and in combinations, to see how their interaction will influence the hydrodynamic coefficients.

Acknowledgment

This work was financed by the Research Council of Norway, NFR project 237929 CRI MOVE.

Nomenclature

d	=	width of plate model (m)
l	=	numerical domain size (m)
n	=	number of periods
p	=	perforation ratio (–)
t	=	plate thickness (mm)
z	=	amplitude of motion (m)
A	=	hydrodynamic mass in vertical direction (kg)
B	=	damping in vertical direction (kg/s)
D	=	total width of model (m)
L	=	length of model (m); $L = 0.57$ m in all experiments
M	=	structure mass in air (kg)
N	=	number of plates
T	=	period of oscillation (s)
W	=	velocity amplitude (m/s)
\ddot{z}	=	acceleration in vertical direction (m/s ²)
\dot{z}	=	velocity in vertical direction (m/s)
A_0	=	infinite fluid added mass for a two-dimensional plate as predicted by potential flow theory (kg)
Re	=	Reynolds number (–)
Δ	=	numerical cell size (m)
Δt	=	time-step size (s)
Δx	=	length of cell in horizontal direction (m)
Δz	=	length of cell in vertical direction (m)
ρ	=	water density (kg/m ³); $\rho = 1000$ kg/m ³ in test tank
ν	=	kinematic viscosity of water (m ² /s); $\nu = 9.55 \times 10^{-7}$ m ² /s at temperature 22 °C
ω	=	frequency of oscillation (rad/s)

References

- 1 Sarpkaya, T., and Isaacson, M., 1981, *Mechanics of Wave Forces on Offshore Structures*, Van Nostrand Reinhold Co. Inc, New York, NY.
- 2 Sumer, B. M., and Fredsøe, J., 1997, *Hydrodynamics Around Cylindrical Structures*. Advanced Series on Ocean Engineering—Volume 12, World Scientific Publishing Co. Pte. Ltd, Singapore.
- 3 Zdravkovich, M. M., 2003, *Flow Around Circular Cylinders*, Oxford University Press.[Q5]
- 4 DNVGL AS. Recommended Practice “Modelling and Analysis of Marine Operations”, DNVGL-RP-N103, July 2017.
- 5 Sandvik, P. C., Solaas, F., and Firoozkoobi, R., 2016, “Hydrodynamic Forces on Complex Subsea Structures,” Marine Operations Specialty Symposium (MOSS 2016), Singapore.
- 6 Mentzoni, F., Abrahamsen-Prsic, M., and Kristiansen, T., 2018, “Hydrodynamic Coefficients of Simplified Subsea Structures,” OMAE2018-78315, Madrid, Spain, June 17-22, 2018.[Q6]
- 7 An, S., and Faltinsen, O. M., 2013, “An Experimental and Numerical Study of Heave Added Mass and Damping of Horizontally Submerged and

- Perforated Rectangular Plates," *J. Fluids Struct.*, **39**, pp. 87–101. [10.1016/j.jfluidstructs.2013.03.004](https://doi.org/10.1016/j.jfluidstructs.2013.03.004)
- 8** Molin, B., 2011, "Hydrodynamic Modelling of Perforated Structures," *Appl. Ocean Res.*, **33**(1), pp. 1–11. [10.1016/j.apor.2010.11.003](https://doi.org/10.1016/j.apor.2010.11.003)
- 9** Chorin, A. J., 1968, "Numerical Solution of the Navier-Stokes Equations," *Math. Comput.*, **22**(104), pp. 745–762. [10.1090/S0025-5718-1968-0242392-2](https://doi.org/10.1090/S0025-5718-1968-0242392-2)
- 10** Mentzoni, F., and Kristiansen, T., 2019, "Numerical Modelling of Perforated Plates in Oscillating Flow," *Appl. Ocean Res.*, **84**, pp. 1–11. [10.1016/j.apor.2018.12.016](https://doi.org/10.1016/j.apor.2018.12.016)**[Q7]**
- 11** Mentzoni, F., and Kristiansen, T., 2019, "A Semi-Analytical Method for Calculating the Hydrodynamic Force on Perforated Plates in Oscillating Flow," Manuscript Submitted for the International Conference on Offshore Mechanics and Arctic Engineering, OMAE2019-95093.
- 12** Tian, X., Tao, L., Li, X., and Yang, J., 2017, "Hydrodynamic Coefficients of Oscillating Flat Plates at $0.15 < KC < 3.15$," *J. Mar. Sci. Technol.*, **22**(1), pp. 101–113. [10.1007/s00773-016-0401-2](https://doi.org/10.1007/s00773-016-0401-2)**[Q8]**